Kinetics for the Partial Oxidation of Methane on a Pt Gauze at Low Conversions

Carlo R. H. de Smet, Mart H. J. M. de Croon, Rob J. Berger, Guy B. Marin, and Jaap C. Schouten
Eindhoven University of Technology, Laboratory of Chemical Reactor Engineering, PO Box 513, 5600 MB Eindhoven, The Netherlands

Intrinsic kinetics of the catalytic partial oxidation of methane were studied at atmospheric pressure in the presence of transport limitations using a single Pt gauze. Catalyst temperature and gas-phase temperatures were measured directly. CO, CO_2, and H_2O were the main products at catalyst temperatures between 1,030 and 1,200 K, residence times of 0.02 to 0.2 ms, CH_4/O_2 ratios between 1.8 and 5.0, and O_2 conversions between 9 and 46%. A kinetic model was developed that consists of six reaction steps. Methane adsorption had to be considered as oxygen-assisted to describe the experimental data, in particular the decrease of the selectivity for CO with increasing space times. Corresponding intrinsic kinetic parameters were obtained from the literature and from regression of the experimental CO selectivities. The calculated conversions and selectivities were obtained using the intrinsic kinetic model, together with a reactor model accounting for no transport limitations quantitatively without any adjustable parameter. Simulations indicate initial CO selectivities between 86 and 96% over the investigated range of conditions, and illustrate the relevance of both surface kinetics and mass transport in CO formation.

Introduction

The availability of large natural-gas resources has been a key driving force in the past years to investigate and develop efficient natural-gas conversion routes for the production of valuable chemicals. At present, commercial processes for natural-gas conversion are mainly based on synthesis gas, that is, a mixture of CO and H_2 (Christensen and Primdahl, 1994). Steam reforming still remains the major industrial route for synthesis-gas production. However, catalytic partial oxidation (CPO) of methane by oxygen has attracted widespread attention as an energy-efficient alternative to steam reforming. Supported transition-metal catalysts (Prettre et al., 1946; Vernon et al., 1990; Vermeiren et al., 1992), as well as noble-metal-based catalysts (Hickman and Schmidt, 1992), have been reported to give high activity and selectivity toward synthesis gas.

On supported transition-metal catalysts, synthesis-gas formation is considered to proceed indirectly, that is, via total oxidation and reforming in series (Prettre et al., 1946; Vernon et al., 1990). At short residence times, using noble-metal catalysts, direct CPO mechanisms were proposed, yielding CO and H_2 in a single step (Hickman and Schmidt, 1992; Mallens et al., 1995). Relatively few studies provide insights into the intrinsic kinetics that determine reactant conversions and synthesis-gas selectivity. Hickman and Schmidt (1993) published detailed elementary-step kinetic models, used to simulate the CPO reaction at high temperatures (1,100–1,500 K) and atmospheric pressure on Pt- and Rh-coated monoliths. The rate parameters of the individual surface reactions were obtained from the literature and from fits to experiments. Analogous elementary-step kinetic models were used to model short-contact-time CPO reactors (Deutschmann et al., 1998) and the ignition behavior of methane/oxygen mixtures (Bui et al., 1997; Deutschmann et al., 1994; Treviño, 1999).

At a methane-to-oxygen ratio of 2 and sufficiently high temperatures, the equilibrium composition corresponds to complete methane and oxygen conversions and 100% selec-

Correspondence concerning this article should be addressed to J. C. Schouten.
Present addresses of: R. J. Berger, Department of Chemical Engineering, Delft University of Technology, Julianalaan 136, 2628 BL Delft, The Netherlands; G. B. Marin, Laboratorium voor Petrochemische Techniek, Universiteit Gent, Krijgslaan 281, S5, B-9000 Ghent, Belgium.

tivity to synthesis gas. This makes the distinction between the direct and indirect formation of synthesis gas difficult. In addition, the kinetics of the catalytic partial oxidation of methane cannot be determined in a straightforward way. First of all, the CPO reaction is extremely fast, which indicates that mass-transport limitations are likely to occur. Also, nonselective, exothermic oxidation reactions can lead to severe heat-transport limitations, resulting in high catalyst temperatures. Heitnes Hofstad et al. (1996) and Hickman and Schmidt (1992) used an optical pyrometer to determine the catalyst temperature at reaction conditions. In most kinetic studies, however, heat-transfer resistances are not taken into account, since only gas-phase temperatures are measured.

Several experimental reactor configurations have been used to study the reaction kinetics of CPO at short residence times and high temperatures. These configuration have in common that, in contrast to fixed beds, the catalytic material is present in a structured way. A catalytic annular reactor was applied by Beretta et al. (1999). To study the intrinsic kinetics of the CPO reaction in the presence of heat-transport limitations, de Smet et al. (1999) developed an experimental reactor, containing a single Pt gauze catalyst. Heat-transport limitations were taken into account explicitly in this reactor, since the catalyst temperature was measured directly, using a thermocouple spot-welded to the Pt gauze. It was demonstrated that experiments could not be performed at conditions where both conversions and selectivities are determined by chemical phenomena alone. Therefore, taking into account the relevant transport phenomena, de Smet et al. (1999) developed a reactor model to obtain the intrinsic kinetic parameters of the CPO reaction on a Pt gauze.

It could be argued that Rh is a better catalyst than Pt for the CPO reaction, especially with respect to hydrogen production. However, experiments performed in our laboratory with Pt–10% Rh gauzes very much resembled the results obtained with Pt gauzes. At conditions of incomplete oxygen conversion and stable catalyst performance, CO, CO_2, and H_2O were always the main products. Hydrogen was not observed at the applied reaction conditions. The main difference between both catalysts was related to stability: the Pt–10% Rh gauze catalyst could be operated at higher temperatures, although hydrogen was still not observed. A disadvantage of the Pt–10% Rh catalyst was the narrow window of operating conditions. The reaction extinguished at relatively high temperatures (approximately 1,073 K), whereas the Pt gauze catalyst remained ignited at temperatures as low as 723 K. Hence, taking into account the small differences in selectivities and the narrow window of operating conditions, Pt was selected as the most suitable catalyst for this kinetic study.

The present article reports on the development of a kinetic model for the catalytic partial oxidation of methane on a single Pt metal gauze, in the presence of irreducible transport phenomena. Experiments were performed in which the influence of the catalyst temperature, the reactant space time, and the inlet methane-to-oxygen ratio was investigated. The experimental data, together with the reactor model presented by de Smet et al. (1999), are used to estimate the corresponding intrinsic kinetic parameters. The objective of the present study is not to provide a fully comprehensive kinetic mechanism that can account for synthesis gas production. The main goal is to obtain the intrinsic kinetics that determine the CO selectivity. Special attention will be paid to primary formation of carbon monoxide, and the importance of mass-transport limitations. Hence, the conversions of methane and oxygen were maintained well below 100%.

Table 1. Range of Experimental Conditions

Catalyst temperature (K)	1,023–1,200
Total pressure (kPa)	130–165
Total flow rate ($mmol \cdot s^{-1}$)	1.5–20
$W/F_{CH_{4,0}}$ ($g \cdot s \cdot mol^{-1}$)	10–130
$CH_4/O_2\|_0$	1.8–5.0
He dilution (%)	35–80
CH_4 conversion	0.02–0.12
O_2 conversion	0.09–0.46

Experimental Equipment, Procedures, and Conditions

The partial oxidation of methane was studied in a continuous-flow-reactor setup containing a single Pt gauze catalyst (150 meshes/cm^2, $W_{cat} = 5.72 \cdot 10^{-2}$ g, $d_w = 0.2$ mm). The reactant gases were preheated and subsequently passed over the Pt gauze catalyst. Heat-transfer resistances were taken into account explicitly, since both the gas-phase temperature and the temperature of the catalyst were measured directly during the experiments. The catalyst temperature was determined by means of a surface thermocouple, constructed by spot-welding a thin Pt–10% Rh wire ($d_w = 0.1$ mm) to the center of the gauze catalyst. An optical pyrometer was used to validate the catalyst temperature measurements and to verify the uniformity of the gauze temperature.

At typical experimental conditions, the measured catalyst temperatures were always significantly higher than the bulk gas-phase temperatures, indicating that strong heat-transfer limitations indeed occur. Consequently, the measured catalyst temperature was used to determine the intrinsic kinetic parameters of the CPO reaction. A total number of 40 experiments was performed at the range of conditions shown in Table 1. Note that the highest oxygen conversion is 46%.

The influence of the reactant space time, $W/F_{CH_{4,0}}$, and the inlet methane-to-oxygen ratio on conversions and selectivities were investigated at a fixed catalyst temperature of 1,123 K. The space time, which is a characteristic measure for residence time at inlet conditions in a fixed-bed reactor configuration, was varied by adjusting the total inlet molar flow rate. The catalyst temperature was kept at a constant value by decreasing the gas preheat temperature at increasing space times and decreasing $CH_4/O_2|_0$ ratios. The influence of the inlet methane-to-oxygen ratio was studied at constant total molar flow rate. The CH_4/O_2 ratio was varied by adjusting both the inlet molar flow rates of methane and helium, since the inlet molar flow rate of oxygen was fixed. Additional details about the experimental equipment and procedures can be found in de Smet et al. (1999).

At the high-temperature conditions applied in this study, gas-phase reactions can become important. Berger and Marin (1999) developed a kinetic model for gas-phase chain reactions at typical CPO conditions. Simulations using this kinetic model, together with a plug-flow reactor model, resulted in very low methane and oxygen conversions. This indicates that

gas-phase reactions can be neglected at the applied conditions. These low conversions are mainly caused by the high total molar flow rates and the low reactant partial pressures applied during the experiments.

Modeling Procedures

Reactor model

To obtain the intrinsic kinetic parameters that determine the CO production rate, the reactor model developed by de Smet et al. (1999) was used. In this reactor model, which takes into account the transport limitations, the complex 3-D geometry of the gauze catalyst was described by two rows of parallel flat plates in series (flat-plate reactor model; see Figure 1). The volumetric surface area and the residence time in case of the actual gauze catalyst, and as applied in the flat-plate reactor model, are required to be identical. Consequently, the characteristic dimensions of the flat-plate reactor model, that is, the distance between the flat plates, h, and the length of the flat plates, b, can be calculated from the gauze wire diameter and the distance between the centers of two wires. The continuity equations account for mass transport by means of axial convection and radial diffusion:

$$\frac{2 \cdot F_{v,b} \cdot h}{A_{\text{cat}}} \cdot \frac{\partial y_i}{\partial z} = D_{m,i}|_{\text{eff}} \cdot \frac{\partial^2 y_i}{\partial r^2}, \tag{1}$$

where z and r correspond to the dimensionless axial and radial coordinates, and $D_{m,i}|_{\text{eff}}$ is the effective diffusion coefficient. The following initial and boundary conditions are used:

$$z = 0 \wedge 0 < r < 1/2: \qquad y_i = y_{i,0} \tag{2}$$

$$z > 0 \wedge r = 0: \qquad \frac{\partial y_i}{\partial r} = 0 \tag{3}$$

$$z > 0 \wedge r = 1/2: \qquad -D_{m,i}|_{\text{eff}} \cdot \frac{C_{t,b}}{h} \cdot \frac{\partial y_i}{\partial r} = r_{i,A}. \tag{4}$$

The mol fraction profiles are symmetric around the radial position $r = 0$. At the catalyst surface, the molar flux is equal to the areal reaction rate, which is governed by the reaction kinetics.

Since the reactant gases are flowing perpendicularly to the wires of the gauze catalyst, complex flow patterns can develop as a function of the Reynolds number (Re). These flow patterns have a strong influence on the heat and mass-transfer rates. In order to account for this influence in the reactor model, the effective diffusion coefficients were calculated using a Sherwood-correlation (Sh) for forced convection of gases to a cylinder in crossflow (Churchill and Bernstein, 1977) and the diffusion coefficient in the absence of convection. In the isothermal case this leads to:

$$Sh = 0.39 + \frac{0.66 \cdot Re^{1/2} \cdot Sc^{1/3}}{\left[1 + (0.4/Sc)^{2/3}\right]^{1/4}} \cdot \left[1 + \left(\frac{Re}{282{,}000}\right)^{5/8}\right]^{4/5} \tag{5}$$

and

$$D_{m,i}|_{\text{eff}} = \frac{\pi^2}{8} \cdot D_{m,i} \cdot \left(\frac{h}{D_{w-w}}\right) \cdot \frac{Sh^2}{Re \cdot Sc}. \tag{6}$$

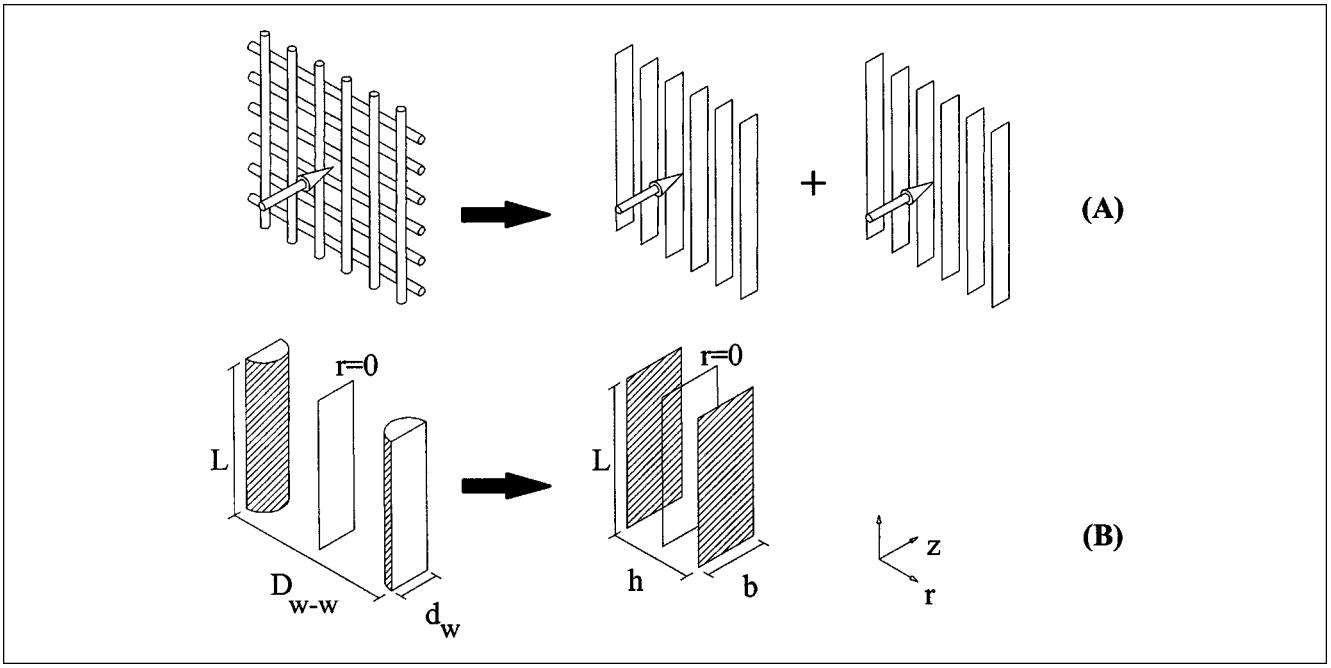

Figure 1. (A) Gauze catalyst and the flat-plate reactor model and (B) the characteristic dimensions of a single row of cylinders of the gauze catalyst and a single row of flat plates in the flat-plate reactor model.

Equation 6 was derived by requiring identical conversions in case of a single row of parallel cylinders and a single row of parallel flat plates (see Figure 1) at total mass-transfer limited conditions.

The set of partial differential equations, together with the initial and boundary conditions, were solved numerically, using the method of lines and the method of Gear in the standard NAG-library routine D03PGF (NAG Fortran Library, 1991). The resulting radial mol-fraction profiles at the reactor outlet were integrated and used to calculate the conversions and selectivities corresponding to a given reactant space time, inlet methane-to-oxygen ratio, and catalyst temperature. The complete derivation of the reactor model and the solution procedure can be found in de Smet et al. (1999). There it is shown that the development of the reactor model was based on Fluent simulations using the full 3-D geometry of the gauze catalyst. The simulations involved solution of the complete Navier-Stokes equations, as well as energy and continuity equations. Surface reaction at the wires of the gauze catalyst was taken into account. Validation of the reactor model was carried out by comparison of the results of the 3-D Fluent simulations with calculated results of the reactor model. This validation was based on different values of inlet velocities, temperatures, surface kinetics, and intrinsic reaction-rate constants. Both gas-phase temperatures and reactant conversions were compared. From parity plots it was evident that the reactor model provides for an excellent description of the gauze reactor.

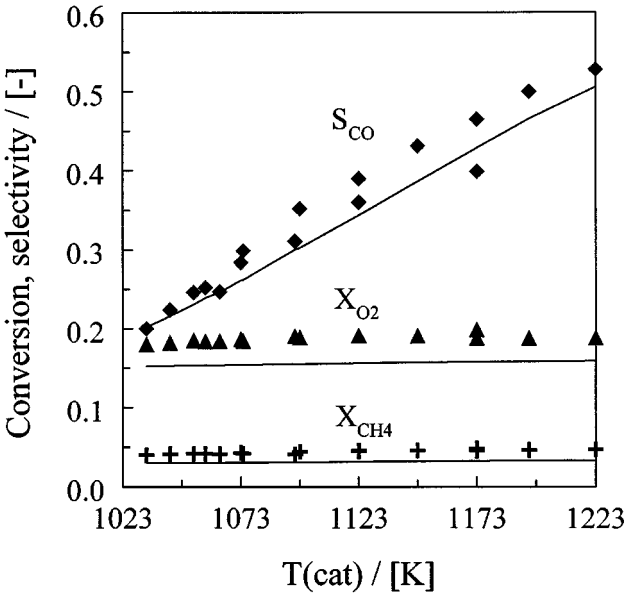

Figure 2. Conversions and selectivities vs. catalyst temperature.

Lines: calculated using the flat-plate reactor model (de Smet et al., 1999) and the kinetic model, with corresponding kinetic parameters listed in Table 2. Points: experiments. Conditions: $P_{tot} = 130$ kPa; $F_{tot} = 1 \times 10^{-2}$ mol·s^{-1}; $W/F_{CH_{4,0}} = 39.9$ g·s·mol^{-1}; $CH_4/O_2/He|_0 = 14.3/5.7/80$.

Parameter estimation

Intrinsic kinetic parameters were estimated by means of nonlinear regression, using a single-response Marquardt-Levenberg algorithm implemented in Odrpack (Boggs et al., 1992). Since the observed methane and oxygen conversions are completely determined by mass transport, the kinetic parameters are obtained from the least-squares criterion, applied to the observed and calculated CO selectivity. The parameter estimates were tested for significance by means of the approximate, individual *t*-values. The statistical significance of the global regression was expressed by means of the *F*-ratio, which is based on the ratio of the mean calculated sum of squares and the mean regression sum of squares. In order to avoid the correlation between the activation energy and the preexponential factor of the methane adsorption-rate coefficient, reparametrization of the Arrhenius equation was applied (Kitrell, 1970):

$$k = A \exp\left(\frac{-E_{act}}{RT_{avg}}\right) \exp\left(\frac{-E_{act}}{R}\left(\frac{1}{T_{cat}} - \frac{1}{T_{avg}}\right)\right), \quad (7)$$

in which T_{avg} is the average catalyst temperature of the experiments ($T_{avg} = 1115$ K). The total number of 40 experiments was used during the regression analysis.

Effects of Reaction Conditions

At the range of conditions investigated, CO, CO_2, and H_2O were the main products. H_2 was found only at catalyst temperatures above 1273 K. At these temperatures, however, the gauze catalyst did not exhibit stable performance with time-on-stream. Platinum deposits were found downstream of the gauze catalyst, as a result of the formation of volatile Pt-oxide species. In addition, a slow increase of the reactant conversions with time-on-stream was observed, which is generally ascribed to morphological changes of the Pt catalyst (Bergene et al., 1996). In order to perform experiments at constant catalyst activity, the catalyst temperature was always kept below 1,200 K. The influence of the catalyst temperature, the reactant space time, $W/F_{CH_{4,0}}$ and the inlet CH_4/O_2 ratio on conversions and selectivities are shown in Figures 2 to 4.

Figure 2 demonstrates that the methane and oxygen conversions are hardly temperature dependent, indicating that the reaction rates are determined by transport phenomena. The selectivity to carbon monoxide, however, varies considerably with catalyst temperature. The CO production rate thus appears to be influenced significantly by the surface chemistry. The measured methane and oxygen conversions increase at increasing reactant space times (see Figure 3). The selectivity to CO decreases at increasing space time, which suggests that CO is a primary product of the oxidation reaction. Figure 4 shows that both the methane and oxygen conversions decrease at increasing CH_4/O_2 ratio. The selectivity to CO increases considerably with an increasing methane-to-oxygen ratio. Similar trends were observed by Hickman and Schmidt (1992), Heitnes Hofstad et al. (1996), and Fahti et al. (1998) using both Pt and Pt–10% Rh gauzes.

Kinetic Model Development

Reaction network

The kinetic model used in this work, which will be referred to as the oxygen-assisted CPO mechanism, is shown in Table

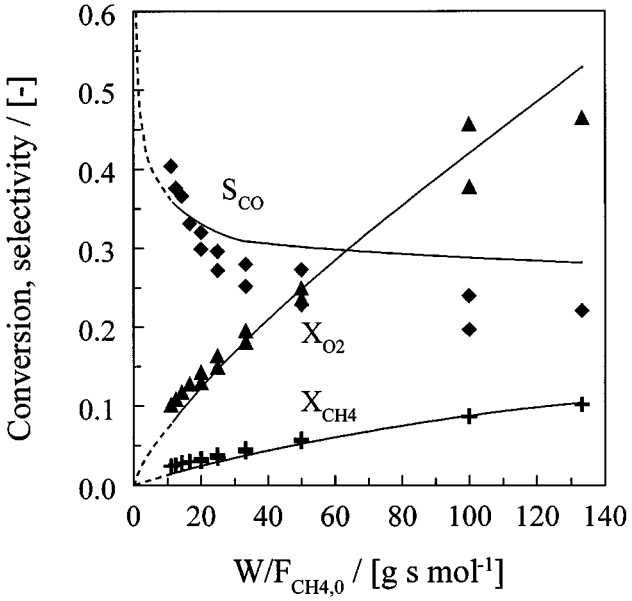

Figure 3. Conversions and selectivities vs. space time.

Full lines: calculated using the flat-plate reactor model (de Smet et al., 1999) and the kinetic model, with corresponding kinetic parameters listed in Table 2. Dashed lines: calculated at low space times, outside the range listed in Table 1. Points: experiments. Conditions: $P_{tot} = 160$ kPa; $T_{cat} = 1{,}123$ K; $CH_4/O_2/He|_0 = 28.6/11.4/60$.

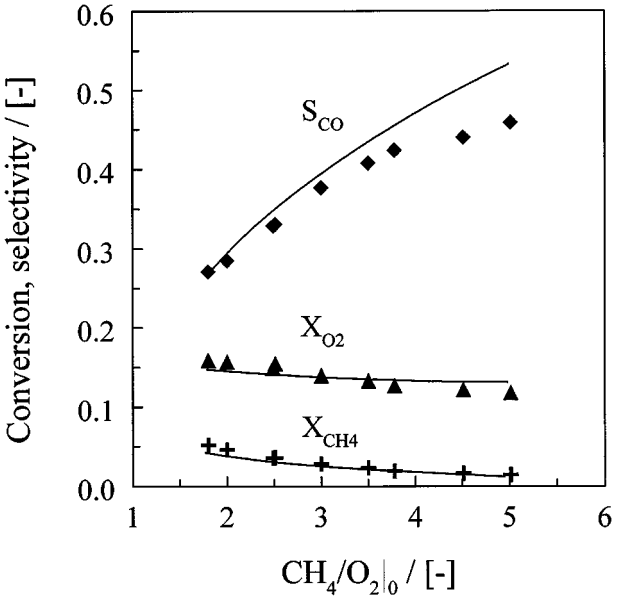

Figure 4. Conversions and selectivities vs. inlet methane-to-oxygen ratio.

Lines: calculated using the flat-plate reactor model (de Smet et al., 1999) and the kinetic model, with corresponding kinetic parameters listed in Table 2. Points: experiments. Conditions: $P_{tot} = 130$ kPa; $T_{cat} = 1{,}123$ K; $F_{tot} = 1 \times 10^{-2}$ mol·s^{-1}; $y_{O_2}|_0 = 0.114$.

2, together with the corresponding rate equations. The mechanism consists of six reaction steps; oxygen and methane adsorption, surface reactions toward CO and CO_2, desorption and adsorption of CO are considered. All reaction steps, with the exception of CO adsorption/desorption, are considered to be irreversible. This is justified, since both the methane and oxygen conversions are considerably lower than 100%. Irreversible methane and oxygen adsorption may lead to a structurally unstable kinetic model, as a result of the occurrence of a transcritical bifurcation point (Nibbelke et al., 1998). Reactor simulations with the kinetic parameters obtained after regression show, however, that these structural instabilities do not occur. This is a result of the low surface coverages of both adsorbed carbon and oxygen species at the conditions investigated.

Oxygen Adsorption. The first step in the reaction mechanism concerns the activation of oxygen through dissociative adsorption. According to Williams et al. (1992), the adsorption rate can be assumed to be first order in the fraction of vacant surface sites θ_*, which implies that the rate-determining step in the adsorption involves the interaction of molecular oxygen with a single catalytic site. Oxygen adsorption is considered to be competitive, in constrast to the mechanism proposed by Hickman and Schmidt (1993). In the latter 19-step mechanism, oxygen is assumed to adsorb on specific catalytic sites, that is, noncompetitively with other species, in order to be able to simulate the experimentally observed O_2 adsorption-limited CO production rate.

Methane Adsorption. Dissociative adsorption of methane, resulting in the formation of a surface carbon species and gaseous water, is taken into account in reaction 2. In agreement with theoretical calculations of Au et al. (1999), methane adsorption under the present conditions is considered to be oxygen-assisted, directly resulting in adsorbed hydroxyl species that recombine instantaneously to gaseous water. Oxygen-assisted methane adsorption is included in the kinetic model to be consistent with the observed decrease of the CO selectivity at increasing space times. This is illustrated later, by examining analytical expressions for the in-

Table 2. Oxygen-Assisted CPO Reaction Mechanism with Corresponding Rate Equations and Kinetic Parameters

No.	Reaction	Rate Equation	A c.q. s_0[§]	E_{act}[‖]	Reference
1	$O_{2,g} + 2* \rightarrow 2O*$	$r_1 = k_1 p_{O_2} \theta_*$	0.023	0	Elg et al. (1997)
2	$CH_{4,g} + 2O* \rightarrow C* + 2H_2O_g + *$	$r_2 = k_2 p_{CH_4} \theta_* \theta_O$	$2.39 \cdot 10^5$	48.2	Present work
3	$C* + O* \rightarrow CO* + *$	$r_3 = k_3 \theta_C \theta_O$	$1 \cdot 10^{13}$	62.8	Hickman and Schmidt (1993)
4	$CO* + O* \rightarrow CO_{2,g} + 2*$	$r_4 = k_4 \theta_{CO} \theta_O$	$1 \cdot 10^{13}$	100	Campbell et al. (1980)
5	$CO* \rightarrow CO_g + *$	$r_5 = k_5 \theta_{CO}$	$1 \cdot 10^{13}$	126	McCabe and Schmidt (1977)
6	$CO_g + * \rightarrow CO*$	$r_6 = k_6 p_{CO} \theta_*$	0.84	0	Campbell et al. (1981)

[§]Units: $Pa^{-1}\ s^{-1}$ (2), s^{-1} (3,4,5).
[‖]Units: kJ mol^{-1}· t-values: $t(A_2 \exp(-E_{act,2}/RT_{avg})) = 37.8$, $t(E_{act,2}) = 5.5$.

trinsic selectivity to CO. In addition, oxygen-assisted methane adsorption is in line with the observation that H_2O is the only hydrogen-containing reaction product at the conditions investigated.

Reaction 2 obviously is not an elementary step, but proceeds through a number of intermediates such as adsorbed CH_x ($x = 1$–3) fragments and adsorbed OH species. Molecular methane adsorption on the Pt surface is considered to be reversible and in quasi equilibrium. The abstraction of the first hydrogen atom by adsorbed oxygen species is considered as the rate-determining step in methane decomposition. The subsequent abstraction of hydrogen atoms from adsorbed CH_x fragments, and the recombination of hydroxyl species to water, are potentially very fast. As a result, no CH_x species appear as surface intermediates in the kinetic model. The global rate coefficient for dissociative adsorption of methane, k_2, is the product of the equilibrium coefficient for molecular adsorption and the rate coefficient of the rate determining step.

Carbon Monoxide and Carbon Dioxide Production. Steps 3 to 6 concern paths toward carbon monoxide and carbon dioxide. Reaction 3 describes the formation of adsorbed CO species, which is generally considered to be very fast (Hickman and Schmidt, 1993). Adsorbed CO species are converted to CO_2 in step 4, which desorbs instantaneously. CO_2 adsorption is not taken into account in the kinetic model, since the heat of adsorption of CO_2 on Pt is very low (Shustorovich, 1990). Finally, CO desorption and adsorption are described in the kinetic model by steps 5 and 6.

Surface species mass balances

The kinetic model as shown in Table 2 involves five molecules and four surface species. The steady-state mass balances for the surface species are written as

$$\text{C-balance:} \quad k_2 p_{CH_4} \theta_* \theta_O - k_3 \theta_C \theta_O = 0 \tag{8}$$

$$\text{O-balance:} \quad 2k_1 p_{O_2} \theta_* - 2k_2 p_{CH_4} \theta_* \theta_O - k_3 \theta_C \theta_O - k_4 \theta_{CO} \theta_O = 0 \tag{9}$$

$$\text{CO-balance:} \quad k_3 \theta_C \theta_O - k_4 \theta_{CO} \theta_O - k_5 \theta_{CO} + k_6 p_{CO} \theta_* = 0 \tag{10}$$

$$\text{Vacant sites:} \quad \theta_C + \theta_O + \theta_{CO} + \theta_* = 1. \tag{11}$$

The terms in Eqs. 8 to 10 are in s^{-1} units. The mass-balances were solved numerically in the flat-plate reactor model, using a modified Newton-Raphson method in the NAG-library routine C05NBF (NAG Fortran Library, 1991). The turnover frequencies of the individual surface steps are used to determine the net areal production and consumption rates of all components. These rates are entered into the flat-plate reactor model, via the boundary condition at the catalyst surface (see Eq. 4).

Consistency of the oxygen-assisted CPO mechanism with experimental results

In order to illustrate the qualitative consistency of the oxygen-assisted CPO mechanism with the observed decrease of the CO selectivity with increasing space time (Figure 3), the intrinsic CO selectivity is considered at given axial reactor coordinate z:

$$S_{CO}|_z^{intr} = \frac{r_5 - r_6}{r_2} = 1 - \frac{r_4}{r_2}. \tag{12}$$

The intrinsic selectivity to CO is thus defined as the ratio of the intrinsic CO production rate to the intrinsic methane disappearance rate. Substitution of the corresponding rate equations results in

$$S_{CO}|_z^{intr} = 1 - \frac{k_4 \theta_{CO} \theta_O}{k_2 p_{CH_4} \theta_* \theta_O} = 1 - \frac{k_4 \theta_{CO}}{k_2 p_{CH_4} \theta_*}. \tag{13}$$

Since both the methane adsorption rate and the CO_2 production rate are proportional to the oxygen surface coverage, the CO selectivity is independent of θ_O. The CO adsorption/desorption reaction is approximately in equilibrium at sufficiently high reactant space times, as will be shown later. As a result, the CO adsorption equilibrium coefficient, equal to $K_{CO,ads} = k_6/k_5 = \theta_{CO}/(\theta_* p_{CO})$, can then be substituted into Eq. 13:

$$S_{CO}|_z^{intr} = 1 - \frac{k_4 K_{CO,ads} p_{CO}}{k_2 p_{CH_4}}. \tag{14}$$

Hence, the intrinsic CO selectivity is determined by (1) the rate coefficients of the CH_4 adsorption and CO_2 production steps; (2) the ratio of the rate coefficients for CO adsorption/desorption; as well as (3) the partial pressures of CO and CH_4 at the catalyst surface. According to Eq. 14, the intrinsic selectivity for CO will decrease at increasing space times, when the ratio of the partial pressures of CO and CH_4 increases.

The measured gas-phase partial pressure of methane, oxygen, and carbon monoxide at the reactor outlet are shown in Figure 5a as a function of space time. These observed partial pressures are bulk values, and therefore only provide an indication of the actual partial pressures at the catalyst surface. The influence of space time on the intrinsic CO selectivity can nevertheless be understood qualitatively. Since methane is present in excess during the experiments, the partial pressure decreases only slightly at increasing space time. The partial pressure of CO increases considerably at increasing space times. As a result, the ratio of the partial pressures of CO and CH_4 (see Figure 5b) increases at increasing space time, and consequently, the intrinsic CO selectivity will decrease (Eq. 14).

Comparison with published kinetic models

In case of dissociative methane adsorption, resulting in adsorbed carbon and hydrogen species without the involvement of O-adatoms, as proposed by Hickman and Schmidt (1993), Bui et al. (1997), and Deutschmann et al. (1998), the CH_4

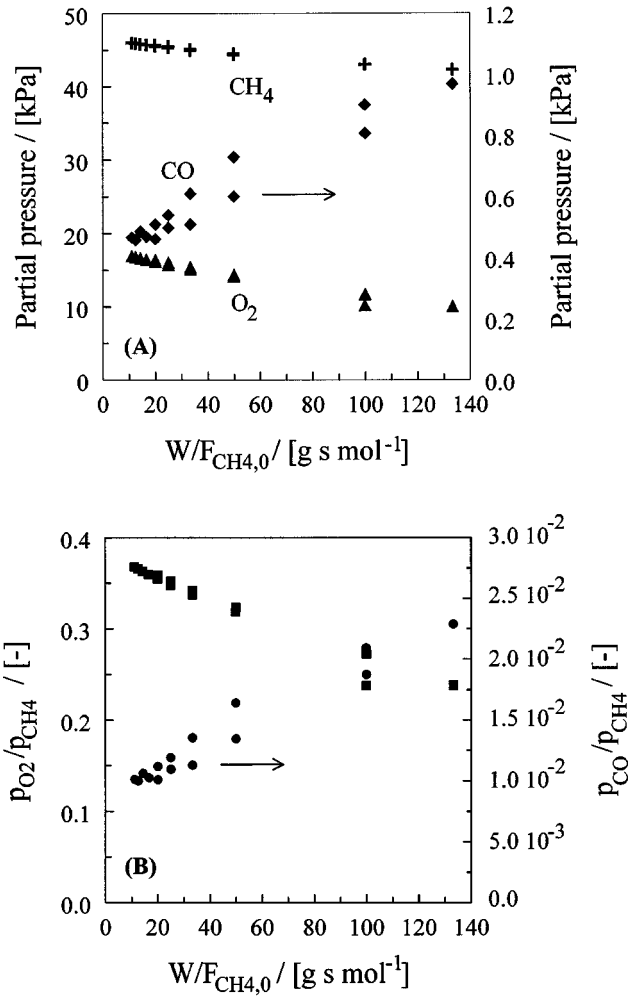

Figure 5. (A) Measured bulk partial pressures and (B) partial pressure ratios at the reactor outlet vs. space time.

Conditions: see Figure 3.

disappearance rate is given by

$$r_2 = k_2 p_{CH_4} \theta_* . \tag{15}$$

The intrinsic CO selectivity then becomes:

$$S_{CO}|_z^{intr} = 1 - \frac{k_4 \theta_{CO} \theta_O}{k_2 p_{CH_4} \theta_*}, \tag{16}$$

and when the CO adsorption/desorption reaction is at quasi-equilibrium:

$$S_{CO}|_z^{intr} = 1 - \frac{k_4 K_{CO,ads} p_{CO} \theta_O}{k_2 p_{CH_4}} . \tag{17}$$

In this case, the intrinsic CO selectivity is also governed by the surface coverage of oxygen. The oxygen surface coverage follows from the steady-state mass balances of adsorbed carbon and oxygen, and can be written in this case as

$$\theta_O = \frac{2k_1 p_{O_2} - 3k_2 p_{CH_4}}{k_4 K_{CO,ads} p_{CO}} . \tag{18}$$

Substitution of Eq. 18 into Eq. 17 results in

$$S_{CO}|_z^{intr} = 4 - 2\frac{k_1 p_{O_2}}{k_2 p_{CH_4}} \tag{19}$$

Because of the stoichiometric excess of methane, the decrease of the partial pressure of O_2 at increasing space time is more pronounced than the decrease of the CH_4 partial pressure (see Figure 5a). The ratio of the partial pressures of oxygen and methane consequently decreases (Figure 5b), and the intrinsic selectivity to CO will *increase* at increasing space times, which is not consistent with the experimental observations. The current analysis thus indicates that the influence of space time on the intrinsic CO selectivity can only be accounted for when methane adsorption is considered to be oxygen-assisted. Dissociative methane adsorption into adsorbed carbon and hydrogen species leads to increasing intrinsic CO selectivities with increasing space time. In addition, simulations with the kinetic model of Hickman and Schmidt (1993) for CPO on Pt, in which dissociative methane adsorption is taken into account, showed that significant amounts of hydrogen are formed even in the presence of nonconverted O_2. This observation is also not consistent with the experimental results.

Kinetic parameter determination

The adsorption rate coefficients of O_2 and CO were calculated from the collision theory:

$$k_{ads,i} = \frac{s_{i,0}}{L_t \sqrt{(2\pi M_i R T_{cat})}} \tag{20}$$

in which $s_{i,0}$ is the initial sticking coefficient, and L_t the total surface concentration of active sites, taken as 1.67×10^{-5} mol $\cdot m_{Pt}^{-2}$. Campbell et al. (1981) investigated CO chemisorption on Pt(111) at 310 K, and reported an initial sticking coefficient of 0.84, which is used in this work. In case of oxygen adsorption on Pt, a wide range of sticking coefficients can be found in the literature. Elg et al. (1997) investigated the temperature dependence of the initial sticking coefficient of oxygen on Pt(111). It was shown that s_0 decreased exponentially from a value of 0.054 at 300 K to 0.023 at 670 K. Here, the high temperature value of 0.023 was used.

The preexponential factors of reactions 3, 4, and 5 were set at a typical value of 10^{13} s^{-1}, which approximately corresponds to the value predicted by transition-state theory (Zhdanov et al., 1988). The corresponding activation energies were taken from the literature (see Table 2). Two kinetic parameters had to be estimated by regression: A and E_{act} of reaction 2. The estimated parameter values, together with the corresponding t-values are shown in Table 2. The t-values indicate that the estimates of the Arrhenius parameters of the methane adsorption are statistically significant. The F-value of the regression amounts to 1,900; the binary correlation coefficient is 0.85. Figure 6 shows a parity plot of the

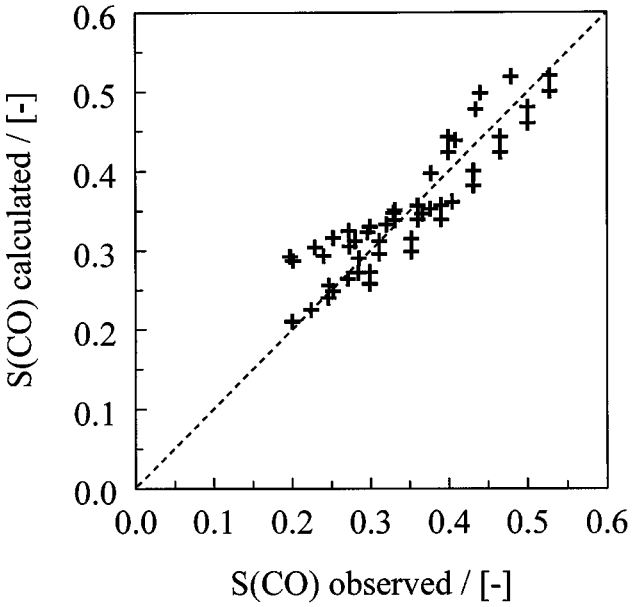

Figure 6. Calculated vs. experimental CO selectivities.

Calculated values obtained with the flat-plate reactor model (de Smet et al., 1999) and the kinetic model, with corresponding kinetic parameters listed in Table 2. Experimental conditions: see Table 1.

experimental and calculated CO selectivities. The deviation between the observed and calculated values is usually within 15%. According to Eq. 14, the intrinsic CO selectivity is governed by the ratio of the rate coefficient of CO_2 production (k_4), the CO adsorption equilibrium coefficient ($K_{CO,ads}$), and the methane adsorption rate coefficient (k_2). Changes in these parameter values mainly affect the absolute value of the CO selectivity. The observed decrease of the selectivity with increasing space times was always observed.

Physicochemical assessment of the parameter estimates

As mentioned earlier, the rate coefficient k_2 is given by the product of the equilibrium coefficient of molecular methane adsorption and the rate coefficient of the rate-determining step, that is, of the hydrogen abstraction from the adsorbed methane molecule by an oxygen adatom. The activation energy of the rate-determining step thus follows from:

$$E_{act,r.d.s.} = E_{act}^{global} - \Delta H_{ads}^{0} \tag{21}$$

in which E_{act}^{global} is the global activation energy of dissociative methane adsorption, and ΔH_{ads}^{0} is the standard adsorption enthalpy of methane. Substitution of the estimated global activation energy, 48.2 kJ mol^{-1}, and the standard adsorption enthalpy of methane, $\Delta H_{ads}^{0} = -25.1$ kJ·mol^{-1} (Shustorovich, 1990), results in an activation energy of the rate-determining step of 73.3 kJ·mol^{-1}. In the literature, no data were found regarding the activation energy of oxygen-assisted methane adsorption. The calculated value, however, is higher than the reported activation energy of 43.1 kJ·mol^{-1} (Anderson and Maloney, 1988) for dissociative methane adsorption into adsorbed carbon and hydrogen species.

The standard activation entropy of the oxygen-assisted methane adsorption reaction can be calculated from the estimated preexponential factor, using

$$A_2 = e\frac{k_b T_{avg}}{h_p}\exp\left(\frac{\Delta^{\#}S_2^{0}}{R}\right), \tag{22}$$

in which A_2 is in bar^{-1} s^{-1} units, that is, with 1 bar as standard pressure. Substitution of the estimated value of A_2 and the average catalyst temperature of the experiments, T_{avg} = 1,115 K, results in $\Delta^{\#}S_2^{0} = -65.6$ J·mol^{-1} K^{-1}. The activation entropy corresponds to the total entropy change in the oxygen-assisted methane adsorption reaction, including both the entropy losses during molecular methane adsorption and the rate-determining step. The standard gas-phase entropy of methane at T_{avg} approximately amounts to 250 J·mol^{-1} K^{-1}. This indicates that the calculated activation entropy is physically realistic, since the methane molecule cannot lose more entropy than it possesses.

Simulation Results and Discussion

Influence of space time

The experimental and simulated conversions and selectivities are shown in Figure 3 as a function of space time. The dashed lines in Figure 3 represent the calculated conversions and selectivities at low $W/F_{CH_{4,0}}$ ratios, outside the experimental range shown in Table 1. Clearly, the measured methane and oxygen conversions are simulated accurately. As indicated before, the oxygen sticking coefficient was fixed at a value of 2.3×10^{-2}. An increase of $s_{O_{2,0}}$ did not result in significantly higher conversions for the mass-transfer limited regime, as expected. The experimentally observed decrease in the CO selectivity with increasing space time is well reproduced by the model. The calculated selectivities, however, are lower than the experimental values at low $W/F_{CH_{4,0}}$ and slightly higher at high $W/F_{CH_{4,0}}$ ratios.

The calculated surface coverage together with the CO and CO_2 production rates at the reactor outlet are shown in Figure 7. The surface coverage of carbon monoxide approximately amounts to 0.15, while the coverages of carbon and oxygen are on the order of 10^{-3}. At increasing space times, the oxygen surface coverage decreases rapidly, as a result of the higher oxygen conversion. The carbon monoxide coverage increases first, and levels off at $W/F_{CH_{4,0}}$ ratios larger than 20 g·s·mol^{-1}. The CO and CO_2 production rates both decrease at increasing space time. However, the decrease of R_{CO} is much more pronounced at low $W/F_{CH_{4,0}}$ ratios, which results in a lower CO selectivity at increasing space time. At $W/F_{CH_{4,0}}$ ratios greater than 20 g·s·mol^{-1}, the ratio between R_{CO} and R_{CO_2} remains approximately constant, and the initial decrease in the CO selectivity is leveled off significantly.

Primary formation of carbon monoxide

Figure 7 indicates that the calculated CO and CO_2 production rates at the catalyst surface are very high, and hence are certainly affected by mass-transport limitations. In order to investigate the influence of the *intrinsic kinetics* on CO formation, calculations were performed at conditions where

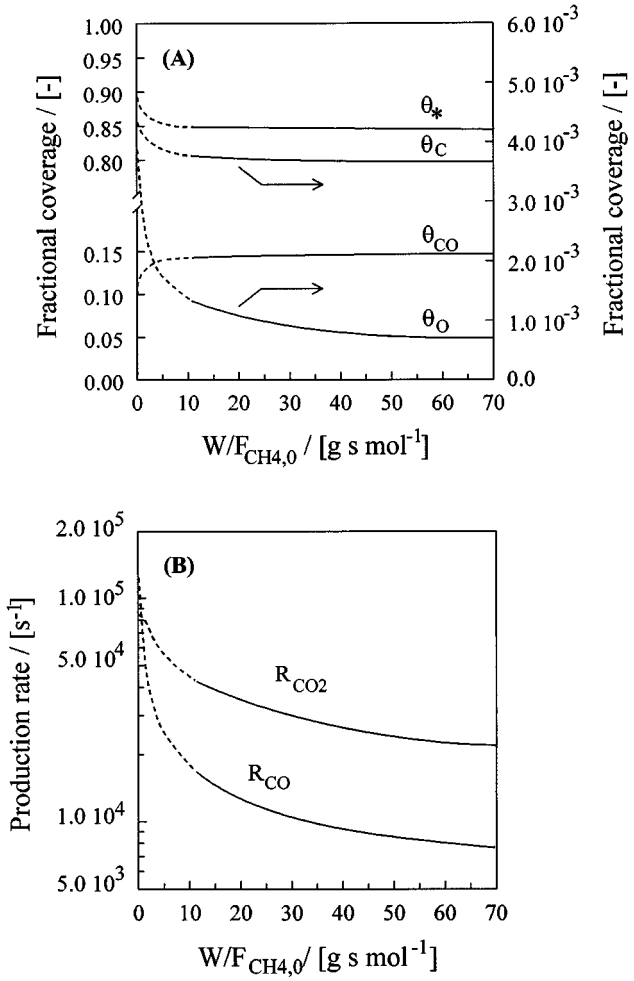

Figure 7. (A) Calculated surface coverages and (B) CO and CO_2 production rates vs. space time.

Dashed lines: simulation results at low space times, outside the range listed in Table 1. Conditions: see Figure 3.

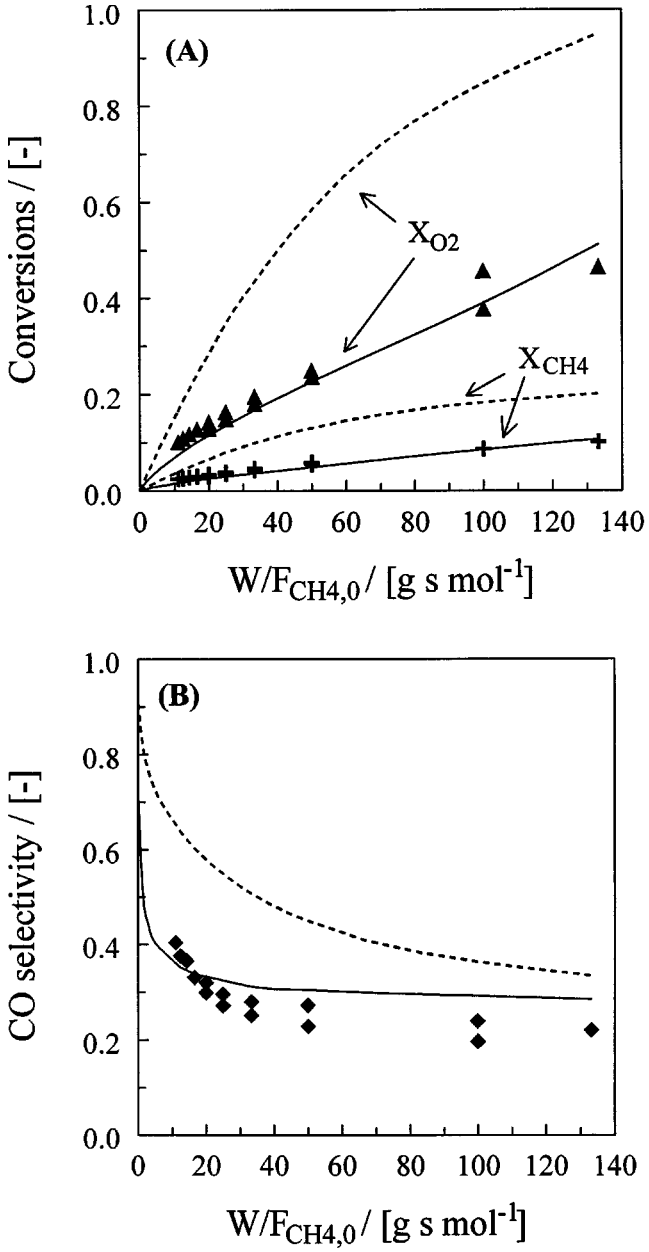

Figure 8. (A) Conversions and (B) selectivities vs. space time.

Full lines: calculated with the flat-plate reactor model (de Smet et al., 1999) and the kinetic model, with corresponding kinetic parameters listed in Table 2. Dashed lines: intrinsic values, calculated by increasing the molecular diffusion coefficients of all gas-phase species with a factor of 10, using the same kinetic model. Points: experimental results. Conditions: see Figure 3.

transport limitations occur for the reactants and products. Intrinsic conversions and selectivities were obtained by increasing the molecular diffusion coefficients of all gas-phase species with a factor of 10, using the kinetic parameters listed in Table 2. A further increase of the molecular diffusion coefficients did not result in significantly higher conversions and selectivities, which indicates that the calculated results indeed correspond to the intrinsic values. The intrinsic conversions and selectivities are shown in Figure 8 as a function of the reactant space time, together with the conversions and selectivities obtained without adjusting the molecular diffusion coefficients.

It is clear that, in the absence of transport limitations, the methane and oxygen conversions are significantly higher than the corresponding values in case of the actual diffusion coefficients. The intrinsic selectivity to CO is also considerably higher than the value calculated without adjusting the diffusion coefficients, but is still decreasing with increasing space times. The decrease of the CO selectivity with increasing space time is evidently caused by the kinetics of the surface reactions. An explanation can be given using the oxygen-assisted CPO reaction mechanism, as shown in Eq. 23:

$$\begin{array}{ccc} CH_{4,g}/O_{2,g} & & CO_g \\ 1\downarrow 2 & & 5\uparrow\downarrow 6 \\ C^* + O^* & \xrightarrow[3]{} & CO^* \xrightarrow[4]{+O^*} CO_{2,g} \end{array} \qquad (23)$$

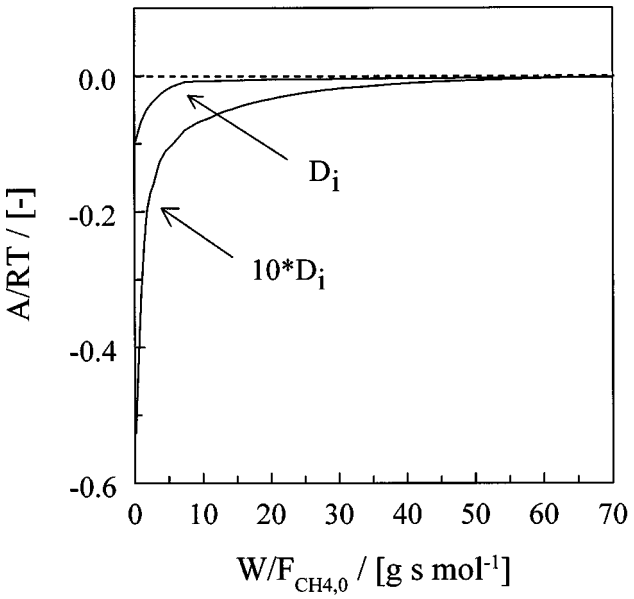

Figure 9. Calculated dimensionless affinity of the CO adsorption/desorption reaction vs. space time.

Conditions: see Figure 3.

At intrinsic conditions, that is, in the absence of mass-transport limitations, the partial pressures of the reactants and products at the catalyst surface are identical to the values in the bulk of the gas phase. At low space times, that is, at low methane and oxygen conversions, the partial pressure of CO is relatively small, as well is the CO adsorption rate (step 6). At increasing $W/F_{CH_{4,0}}$ ratios, the CO partial pressure increases, thus enhancing the CO adsorption rate. This is also reflected in Figure 9, in which the dimensionless affinity of the CO adsorption/desorption reaction is plotted at intrinsic conditions as a function of space time. The dimensionless affinity is obtained from

$$\frac{A}{RT_{cat}} = \ln\left(\frac{r_6}{r_5}\right), \tag{24}$$

and is a measure of the degree at which the CO adsorption/desorption equilibrium is approached. At low $W/F_{CH_{4,0}}$ ratios, the dimensionless affinity is relatively high, which indicates that the CO adsorption/desorption reaction is reversible, but not at equilibrium. At these conditions, the intrinsic selectivity to CO is given by Eq. 13. At increasing values of the reactant space time, the dimensionless affinity decreases rapidly as the CO adsorption/desorption equilibrium is approached. At $W/F_{CH_{4,0}}$ ratios larger than 25 g·s·mol^{-1} the CO adsorption reaction is within 2.5% of its equilibrium. At these space times, the intrinsic selectivity to CO is given by Eq. 14. The observed decrease of the CO selectivity at increasing space times is thus caused by the asymptotic approach of the CO adsorption/desorption reaction toward its equilibrium.

Figure 9 also indicates that the dimensionless affinity in the case of the actual diffusion coefficients is much smaller than the affinity corresponding to the intrinsic situation. This is evidently caused by mass-transport limitations for CO at these conditions. As a consequence of these transport limitations, the CO partial pressure at the catalyst surface is considerably higher than the bulk partial pressure. The CO adsorption rate is thus much higher than in the case of the intrinsic regime, which results in lower selectivities to CO. In addition, Figure 9 indicates that the CO adsorption equilibrium is already reached at much lower space times. As a result, the decrease in the CO selectivity with increasing space times is much more pronounced, and is leveled off significantly at high space times.

Initial CO selectivity

Figure 8 indicates that high CO selectivities are calculated at low values of the reactant space time. At these conditions, the CO adsorption/desorption reaction is reversible, but not in equilibrium. The intrinsic CO selectivity can thus be represented by Eq. 13. This equation can be used to calculate the value of the initial CO selectivity, that is, the selectivity at $W/F_{CH_{4,0}} = 0$. At this $W/F_{CH_{4,0}}$ ratio, CO adsorption can be neglected. The ratio of the surface coverages of adsorbed CO and vacant sites (see Eq. 13) can now be solved analytically, using the steady-state balances for adsorbed C, O, and CO species:

$$S_{CO}|_{ini}^{intr} = 1 - \frac{k_4}{k_2 p_{CH_4}}\frac{\theta_{CO}}{\theta_*} = \frac{5}{2} + \alpha - \sqrt{\left\{\left(\frac{3}{2}+\alpha\right)^2 + 2\alpha\right\}} \tag{25a}$$

in which

$$\alpha = \frac{k_1 k_4}{k_2 k_5}\frac{p_{O_2}}{p_{CH_4}}. \tag{25b}$$

Substitution of the corresponding rate coefficients and inlet partial pressures of methane and oxygen results in an initial CO selectivity of 0.93 at the conditions applied during the $W/F_{CH_{4,0}}$ experiments. The minimum value of the initial CO selectivity is found at a catalyst temperature of 1023 K and inlet methane-to-oxygen ratio of 2.5, and corresponds to 0.86, while a maximum value of 0.96 is found at 1123 K and an inlet methane-to-oxygen ratio of 5. Obviously, CO_2 is produced over the entire range of $W/F_{CH_{4,0}}$ ratios. However, the analysis does show that CO is the most important primary product.

Influence of catalyst temperature

The experimental and simulated conversions and selectivities as a function of the catalyst temperature are shown in Figure 2, at a $W/F_{CH_{4,0}}$ ratio of 40 g·s·mol^{-1}. As expected for a mass-transfer limited regime, the calculated conversions are hardly influenced by the catalyst temperature. The simulated conversions are slightly lower than the experimentally observed values. The observed increase in the CO selectivity at increasing catalyst temperature is predicted accurately. This observation clearly indicates that the kinetics of the sur-

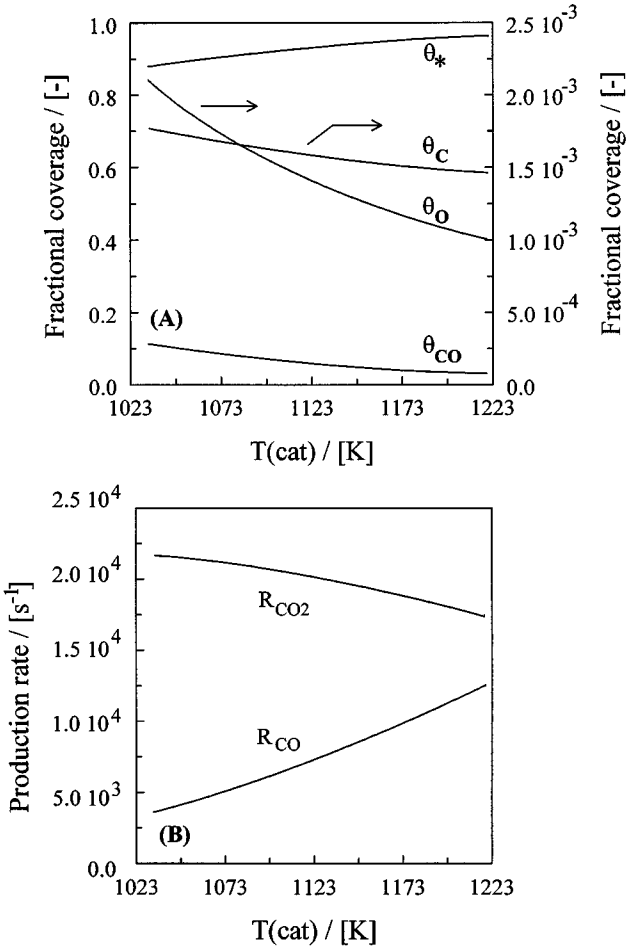

Figure 10. (A) Calculated surface coverages and (B) CO and CO_2 production rates vs. catalyst temperature.

Conditions: see Figure 2.

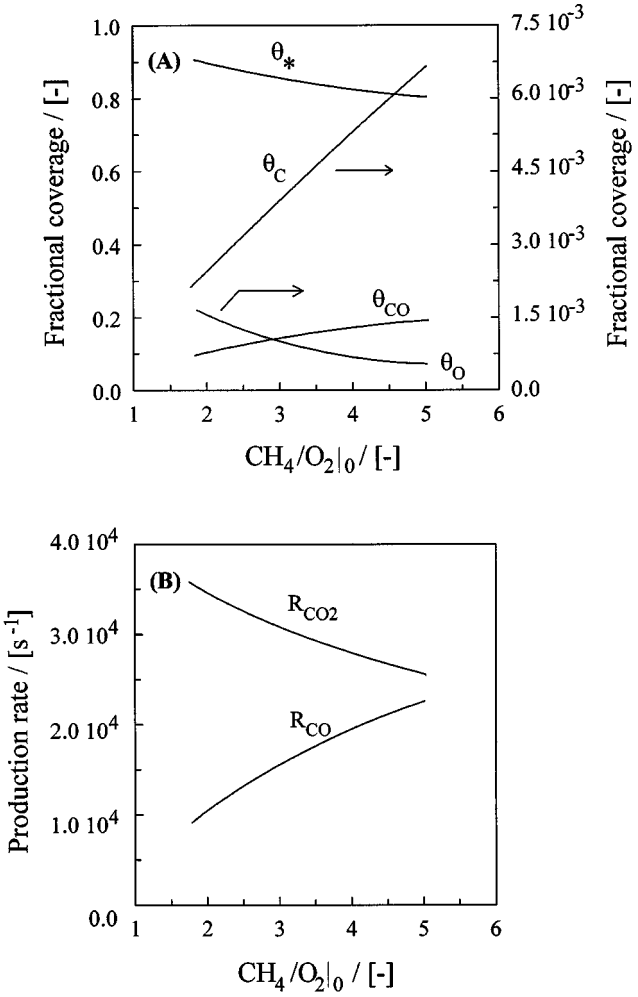

Figure 11. (A) Calculated surface coverages and (B) CO and CO_2 production rates vs. inlet methane-to-oxygen ratio.

Conditions: see Figure 4.

face reactions are indeed crucial in determining the absolute value of the CO production rate.

The corresponding surface coverages, together with the CO and CO_2 production rates as a function of the catalyst temperature, are shown in Figure 10. At increasing temperature, the desorption rate of CO is considerably enhanced, resulting in a decrease in the surface coverages of C, O, and CO. The CO_2 production rate decreases slightly at increasing catalyst temperatures. This is mainly caused by the large decrease in the oxygen surface coverage. At increasing temperature, R_{CO} increases rapidly: the decrease of the CO surface coverage with increasing temperature is obviously more than compensated by the large increase in the CO desorption-rate coefficient. As a result of the increase in the CO production rate, and the decreasing CO_2 production rate, the selectivity to CO increases at increasing catalyst temperatures (Figure 2).

Influence of CH_4/O_2 ratio

Figure 4 demonstrates that the effect of the inlet methane-to-oxygen ratio on the conversions and selectivities is also accurately simulated. The corresponding calculated surface coverages and the production rates of CO and CO_2 at the reactor outlet are shown in Figure 11 as a function of $CH_4/O_2|_0$. At increasing methane-to-oxygen ratios, the surface coverages of adsorbed carbon and carbon monoxide increase, while the coverages of oxygen and vacant surface sites decrease. The increase in the surface coverage of adsorbed carbon is mainly caused by the increase in the CH_4 partial pressure at increasing methane-to-oxygen ratios. The decrease of the oxygen surface coverage is more pronounced than the increase of the CO coverage, which results in decreasing CO_2 production rates at increasing CH_4/O_2 ratios. The CO production rate, however, increases at increasing CH_4/O_2 ratios, which results in the observed increase of the CO selectivity.

Conclusions

The catalytic partial oxidation of methane was studied at atmospheric pressure on a single Pt gauze catalyst. The structured laboratory reactor proved to be a valuable experimental tool for determining the *intrinsic kinetics* of the CPO reaction, as the *catalyst temperature* was measured directly. It was

shown that CO, CO_2, and H_2O were the main products at oxygen conversions lower than 100%. Both the methane and oxygen conversion rates were determined by mass transport, whereas the selectivity to CO was also influenced significantly by the kinetics of the surface reactions.

A kinetic model consisting of six reactions among five molecules and four surface intermediates was developed to describe the experimental observations. Oxygen-assisted methane adsorption was shown to be consistent with the experimental results. In order to obtain the corresponding kinetic parameters, a reactor model without adjustable parameters was applied that takes into account the mass-transport phenomena in a quantitative way. Single-response regression, applied to the observed CO selectivity resulted in statistically significant and physically meaningful estimates of the *intrinsic* kinetic rate parameters of the methane adsorption.

The effects of catalyst temperature, reactant space time, and inlet methane-to-oxygen ratio on the conversions and selectivities could be simulated adequately by the model. The modeling results indicate initial CO selectivities between 0.86 and 0.96. In addition, the present work *quantitatively* illustrates the role of surface kinetics and mass transfer in CO formation.

Acknowledgment

The financial support provided by the Commission of the European Union in the framework of the Joule project, Contract Nos. JOU2-CT92-0073 and JOU3-CT95-0026, as well as the Copernicus Project, Contract No. 41GO4597, is gratefully acknowledged by the authors.

Notation

A_{cat} = catalyst surface area, m^2
$C_{t,b}$ = total concentration at bulk conditions, $mol \cdot m^{-3}$
d_w = wire diameter, m
$D_{w\text{-}w}$ = distance between the centers of two wires, m
E_{act} = activation energy, $kJ \cdot mol^{-1}$
$F_{CH_4,0}$ = inlet molar flow rate of CH_4, $mol \cdot s^{-1}$
$F_{v,b}$ = volumetric flow rate at bulk conditions, $m^3 \cdot s^{-1}$
h_p = Planck constant, $= 6.6262 \times 10^{-34}$ J·s
k_b = Boltzmann constant, $= 1.3807 \times 10^{-23}$ $J \cdot K^{-1}$
k_i = reaction-rate parameter, s^{-1}, $s^{-1} \cdot Pa^{-1}$
M_i = molecular mass, $kg \cdot mol^{-1}$
p_i = partial pressure, Pa
$r_{i,A}$ = areal reaction rate, $mol \cdot m^{-2} \cdot s^{-1}$
R = gas constant, $J \cdot mol^{-1} \cdot K^{-1}$
R_j = net production rate, s^{-1}
$\Delta^{\#}S^0$ = standard activation entropy, $J \cdot mol^{-1} \cdot K^{-1}$
Sc = Schmidt number
T_{cat} = catalyst temperature, K
W_{cat} = catalyst mass, g
X_{CH_4} = conversion of methane
X_{O_2} = conversion of oxygen
y_i = mol fraction
α = parameter

Subscripts

0 = inlet
ini = initial

Literature Cited

Anderson, A. B., and J. J. Maloney, ''Activation of Methane on Iron, Nickel, and Platinum Surfaces. A Molecular Orbital Study,'' *J. Phys. Chem.*, **92**, 809 (1988).

Au, C.-T., C.-F. Ng, and M.-S. Liao, ''Methane Dissociation and Syngas Formation on Ru, Os, Rh, Ir, Pd, Pt, Cu, Ag and Au: A Theoretical Study,'' *J. Catal.*, **185**, 12 (1999).

Beretta, A., P. Baiardi, D. Prina, and P. Forzatti, ''Analysis of a Catalytic Annular Reactor for Very Short Contact Times,'' *Chem. Eng. Sci.*, **54**, 765 (1999).

Bergene, E., O. Trondstad, and A. Holmen, ''Surface Areas of Pt-Rh Catalyst Gauzes Used for Ammonia Oxidation,'' *J. Catal.*, **160**, 141 (1996).

Berger, R. J., and G. B. Marin, ''Investigation of Gas-Phase Reactions and Ignition Delay Occurring at Conditions Typical for Partial Oxidation of Methane to Synthesis Gas,'' *Ind. Eng. Chem. Res.*, **38**, 2582 (1999).

Boggs, P. T., R. H. Byrd, J. E. Rogers, and R. B. Schnabel, *Odrpack Version 2.01, Software for Weighted Orthogonal Distance Regression*, National Institute of Standards and Technology, Gaithersburg, MD (1992).

Bui, P. A., D. G. Vlachos, and P. R. Westmoreland, ''Catalytic Ignition of Methane/Oxygen Mixtures Over Platinum Surfaces: Comparison of Detailed Simulations and Experiments,'' *Surf. Sci.*, **385**, L1029 (1997).

Campbell, C. T., G. Ertl, H. Kuipers, and J. Segner, ''A Molecular Beam Study of the Catalytic Oxidation of CO on a Pt(111) Surface,'' *J. Phys. Chem.*, **73**, 5862 (1980).

Campbell, C. T., G. Ertl, H. Kuipers, and J. Segner, ''A Molecular Beam Investigation of the Interactions of CO with a Pt(111) Surface,'' *Surf. Sci.*, **107**, 207 (1981).

Christensen, T. S., and I. I. Primdahl, ''Improve Syngas Production Using Autothermal Reforming,'' *Hydrocarbon Process.*, **73**(3), 39 (1994).

Churchill, S. W., and M. Bernstein, ''A Correlating Equation for Forced Convection from Gases and Liquids to a Circular Cylinder in Cross Flow,'' *J. Heat Trans.*, **99**, 399 (1977).

De Smet, C. R. H., M. H. J. M. de Croon, R. J. Berger, G. B. Marin, and J. C. Schouten, ''An Experimental Reactor to Study the Intrinsic Kinetics of the Catalytic Partial Oxidation of Methane in the Presence of Heat-Transport Limitations,'' *Appl. Catal. A.*, **187**, 33 (1999).

Deutschmann, O., F. Behrendt, and J. Warnatz, ''Modeling and Simulation of Heterogeneous Oxidation of Methane on a Platinum Foil,'' *Catal. Today*, **21**, 461 (1994).

Deutschmann, O., and L. D. Schmidt, ''Modeling the Partial Oxidation of Methane in a Short-Contact-Time Reactor,'' *AIChE J.*, **44**, 2465 (1998).

Elg, A.-P., F. Eisert, and A. Rosén, ''The Temperature Dependence of the Initial Sticking Probability of Oxygen on Pt(111) Probed with Second Harmonic Generation,'' *Surf. Sci.*, **382**, 57 (1997).

Fathi, M., K. Heitnes Hofstad, T. Sperle, O. A. Rokstad, and A. Holmen, ''Partial Oxidation of Methane to Synthesis Gas at Very Short Contact Times,'' *Catal. Today*, **42**, 205 (1998).

Heitnes Hofstad, K., O. A. Rokstad, and A. Holmen, ''Partial Oxidation of Methane Over Platinum Metal Gauze,'' *Catal. Lett.*, **36**, 25 (1996).

Hickman, D. A., and L. D. Schmidt, ''Synthesis Gas Formation by Direct Oxidation of Methane Over Pt Monoliths,'' *J. Catal.*, **138**, 267 (1992).

Hickman, D. A., and L. D. Schmidt, ''Steps in CH_4 Oxidation on Pt and Rh Surfaces: High-Temperature Reactor Simulations,'' *AIChE J.*, **39**, 1164 (1993).

Kitrell, J. R., ''Mathematical Modelling of Chemical Reactions,'' *Adv. Chem. Eng.*, **8**, 97 (1970).

Mallens, E. P. J., J. H. B. J. Hoebink, and G. B. Marin, ''An Investigation on the Reaction Mechanism for the Partial Oxidation of Methane to Synthesis Gas Over Platinum,'' *Catal. Lett.*, **33**, 291 (1995).

McCabe, R. W., and L. D. Schmidt, ''Binding States of CO and H_2 on Clean and Oxidized (111) Pt,'' *Surf. Sci.*, **65**, 189 (1977).

NAG, Numerical Algorithm Group, *Fortran Library Manual, Mark 15*, Wilkinson House, Oxford (1991).

Nibbelke, R. H., J. H. B. J. Hoebink, M. H. J. M. de Croon, and G. B. Marin, ''Structural Stability of Kinetic Models: Anomalies Due to Irreversible Adsorption,'' *AIChE J.*, **44**, 937 (1998).

Prettre, M., C. Eichner, and M. Perrin, ''The Catalytic Oxidation of

Methane to Carbon Monoxide and Hydrogen,'' *Trans. Faraday Soc.*, **43**, 335 (1946).
Shustorovich, E., ''The Bond-Order Conservation Approach to Chemisorption and Heterogeneous Catalysis: Applications and Implications,'' *Adv. Catal.*, **37**, 101 (1990).
Treviño, C., ''Analysis for the Catalytic Ignition of Methane in a Stagnation Point Flow,'' *AIChE J.*, **45**, 567 (1999).
Vermeiren, W. J. M., E. Blomsma, and P. A. Jacobs, ''Catalytic and Thermodynamic Approach of the Oxyreforming of Methane,'' *Catal. Today*, **13**, 427 (1992).
Vernon, P. D. F., M. L. H. Green, A. K. Cheetham, and A. T. Ashcroft, ''Partial Oxidation of Methane to Synthesis Gas,'' *Catal. Lett.*, **13**, 181 (1990).
Williams, W. R., C. M. Marks, and L. D. Schmidt, ''Steps in the Reaction $H_2 + O_2 \leftrightarrow H_2O$ on Pt: OH Desorption at High Temperatures,'' *J. Phys. Chem.*, **96**, 5922 (1992).
Zhdanov, V. P., J. Pavlícek, and Z. Knor, ''Pre-Exponential Factors for Elementary Surface Processes,'' *Catal. Rev.-Sci. Eng.*, **30**, 501 (1988).

Manuscript received Sept. 13, 1999, and revision received Apr. 3, 2000.